Soft Matter

Supplementary Information

On the Role of Flexibility in Linker-Mediated DNA Hydrogels (SI)

Iliya D. Stoev, *[a] Tianyang Cao, *[b] Alessio Caciagli, [a] Jiaming Yu, [a] Christopher Ness, [c] Ren Liu, [a] Rini Ghosh, [a] Thomas O'Neill, [a] Dongsheng Liu [b] and Erika Eiser ‡[a]

Received:

Accepted:

DOI:

www.rsc.org/

Three-dimensional DNA networks, composed of tri- or higher valent nanostars with sticky, single-stranded DNA overhangs, have been previously studied in the context of designing thermally responsive, viscoelastic hydrogels. In this work, we use linker-mediated gels, where the sticky ends of two trivalent nanostars are connected through the complementary sticky ends of a linear DNA duplex. We can design this connection to be either rigid or flexible by introducing flexible, non-binding bases. The additional flexiblity provided by these non-binding bases influences the effective elasticity of the percolating gel formed at low temperatures. Here we show that by choosing the right length of the linear duplex and non-binding flexible joints, we obtain a completely different phase behaviour to that observed for rigid linkers. In particular, we use dynamic light scattering as microrheological tool to monitor the self-assembly of DNA nanostars with linear linkers as a function of temperature. While we observe classical gelation when using rigid linkers, the presence of flexible joints leads to a cluster fluid with a much-reduced viscosity. Using both the oxDNA model and a coarse-grained simulation to investigate the nanostar-linker topology, we hypothesise on the possible structure formed by the DNA clusters. Moreover, we present a systematic study of the strong viscosity increase of aqueous solutions in the presence of these DNA building blocks.

DNA characterisation

UV-visible spectroscopy

In the sample preparation for UV-visible spectroscopy, the concentrated samples of single-stranded DNA (ssDNA) were diluted down to 1 µM to ensure absorption values between 0.5 and 1.0 at wavelength of 260 nm. We used a UV-visible spectrophotometer (Cary 300 Bio, Agilent Technologies) with temperature control. Only quartz cuvettes were used, and all measured samples were calibrated against a pure phosphate buffer saline solution (100 mM NaCl). The heating or cooling rates were 0.2°C/min, ensuring equilibrium hybridisation.

The melting curves in Figure S1 show the temperature behaviour of the Y-shapes and linkers. We make use of the difference in absorption strength between dsDNA and ssDNA at 260 nm. At high temperatures, we only find ssDNAs, which is why the absorption is at its maximum. As we lower the temperature, the ssDNAs start to hybridise forming duplexes and trivalent nanostars, respectively. The inflection points of the absorption curves are defined as the melting transition of the DNA nanostars and correspond to the temperature, at which about half of all possible hydrogen bonds have formed. [1]

Further decrease in temperature leads to complete hybridisation of our Y-shapes and linkers. The melting temperatures, here extracted at 50% absorption in the normalised UV-vis spectra, are $T_{m,Y}$ = 55°C and $T_{m,L0/6} \approx$ 65°C. These values are close to 52°C and 62°C, evaluated using SantaLucia's data. [2] Note that $T_{m,Y}$ is based on the average melting temperature of the 3 different arms, whose 14 base pairs were designed to have similar melting temperature, but distinguished sequences. The weak hysteresis between heating and cooling data lies within the resolution of our measurement. In our microrheology measurements on hydrogels, we used thousand-fold higher DNA concentrations (which cannot be measured in UV-vis spectroscopy). This large concentration increase leads to a shift of $T_{m,Y}$ and $T_{m,L0(6)}$ by about 5-8°C, as demonstrated earlier.[3] The SantaLucia value for the 12-base sticky overhangs was about 40.5°C for 0.1 M added NaCl and a DNA concentration of 1 µM, meaning in the hydrogel measurements it was shifted to about 48°C. Therefore, we chose to perform our DLS measurements in the 60°C-40°C range.

Polyacrylamide gel electrophoresis (PAGE)

We used a BioRad Mini-PROTEAN tetra cell handcasting accessory kit for performing polyacrylamide gel electrophoresis. The composition of the gel was 10%w PAGE and 11 mM $MgCl_2$ in 1xTE (10 mM tris-HCl and 1mM EDTA) buffer. The target concentration for each DNA strand was around 1 µM. A 2-log DNA ladder (100-10,000 bases, BioLabs, New England) was used as marker. Purple gel-loading dye (6x, BioLabs, New England) facilitated sample loading of the DNA solutions. The tetra cell unit was run at 100 V for 90 min. GelRed (3x, Thermo Fisher Scientific) was used for staining the final gel and a

a.Cavendish Laboratory, Department of Physics, University of Cambridge, Cambridge, CB3 0HE, United Kingdom.
b.Department of Chemistry, University of Tsinghua, Beijing, 100084, China.
c.Department of Chemical Engineering and Biotechnology, University of Cambridge, Cambridge CB3 0AS, United Kingdom.
*Authors with equal contribution.
‡ Corresponding author: ee247@cam.ac.uk.
Electronic Supplementary Information (ESI) available:

Benchtop UV Transilluminator (MultiDoc-It Digital Imaging System, UVP) was used for visualisation.

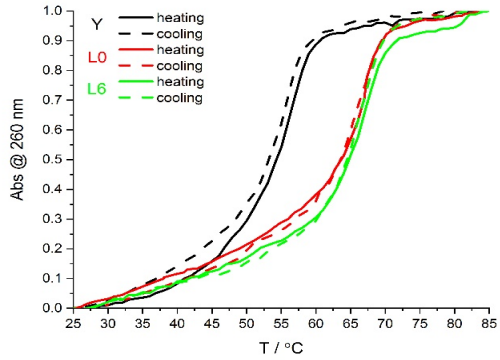

Fig. S1 Normalised absorption at 260 nm for trivalent nanostars (Y-shapes, black) and bivalent duplexes (linear and flexible linkers, red and green, respectively) as a function of temperature. We probe the hysteresis in melting at 100 mM NaCl by measuring both heating (solid curves) and cooling (dashed curves) ramps.

(a)

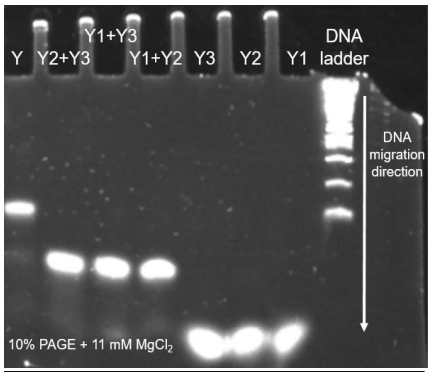

(b)

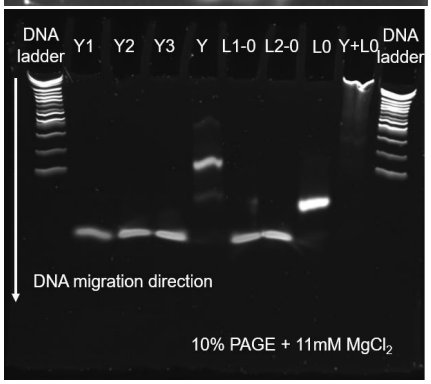

(c)

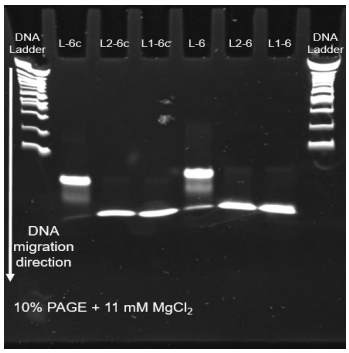

Fig. S2 PAGE on the strands making up (a) the Y-shapes (Y1, Y2 and Y3), (b) linear linkers (L0) without, and (c) flexible linkers (L6) with a 6T joint and L6c, with a shorter linear duplex.. In all gels, we used 2-log DNA ladder as a marker in the terminal columns. The divisions on the DNA ladder range from 100 bases to 10,000 bases.

The images of the gels can be seen in Figure S2: separate ssDNAs Y1, Y2, Y3, L1-0, L2-0, L1-6, L2-6, L1-6c and L2-6c (shortened versions of their L6 counterparts) propagated the longest distance through the porous gel, as expected. The partial complementarity of Y1, Y2 and Y3 as well as the formation of the Y-shape are evident from Figure S2a. Each arm of our Y-shapes is composed of either Y1 and Y2, Y1 and Y3, or Y2 and Y3. The gels demonstrate the successful formation of each arm as well as the high purity of the ssDNAs as evidenced by the very sharp bands. The weaker sidebands for the left 4 columns in Figure S2a are to be expected and are purely due to the slight mismatch in concentration between the three ssDNAs forming the Y-shapes.

Similar purity is obtained for the linear linkers in Figure S2b. We have also included a small low-concentration sample of our hydrogel (Y+L0) as a further proof that the sticky ends between the Y-shapes and the linkers indeed bind. Indeed, the hydrogel did not diffuse at all through the matrix, remaining stuck in place in the gel, close to the well, where it was inserted.

In Figure S2c, we provide proof for the formation of a DNA duplex when using flexible linkers. The L6 linkers, hybridise successfully when combined in equimolar quantities. The slight smearing of the band indicates the presence of free linker strands or slight impurities. Similarly, we show the binding between flexible linkers L6c, which have a shortened hybridising segment compared to L6 due to the deletion of six bases. Due to their smaller size, the strands are observed to reach slightly longer diffusion paths, leaving bands positioned further away from the loading wells. We did not use these L6c linkers in the present study. Combining our PAGE data with the melting curves obtained in UV-visible spectroscopy, we conclude that the strands indeed have the right intended sequences as dictated by their design.

Dynamic light scattering (DLS)

Rigid linkers

In addition to the electric-field autocorrelation functions displayed in the main body of the paper, we show a comparison between the mean-squared displacement (MSD) of our PS-PEG colloids in different concentrations of rigid-linker hydrogels. Figure S3 shows successively the MSDs for colloids in 0.8%w, 1.0%w, 1.6%w and 2.0%w. The temperature range studied is between 60°C and 40°C, which, based on Santa Lucias' next-neighbour model, includes the melting temperature $T_{m,YL0} \approx$ 52-54°C of our hydrogel.

The general trend we observe in each set of MSD curves is a shift towards longer lag times on decreasing the temperature. This is associated with an increased viscosity of the probed sample, up to the point where we form a percolating gel provided the DNA concentration is sufficiently high. While at 60°C the 0.8%w hydrogel sample appears very dilute, it displays a notably different viscosity transitioning from 1.0%w to 1.6%w. In addition, we observe the appearance of a plateau in the MSD suggesting that the colloids are kinetically trapped on intermediate timescales. The temperature, at

which we observe this feature, represents the onset of gel formation and is around 52°C.

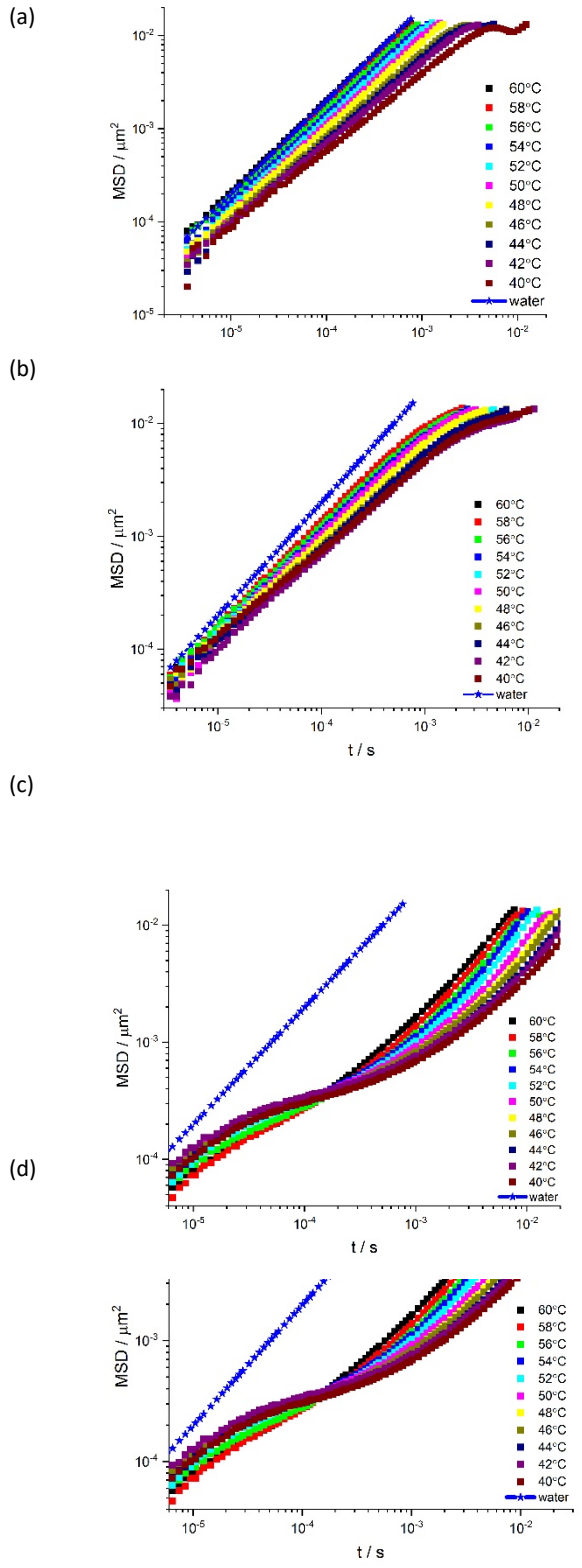

Fig. S3 Ensemble-averaged MSDs for PS-PEG colloids suspended in (a) 0.8%w, (b) 1.0%w, (c) 1.6%w and (d) 2.0%w hydrogels made of 2:3 ratios of Y-shapes and rigid L0 linkers. The curves are plotted as functions of lag time for different temperatures.

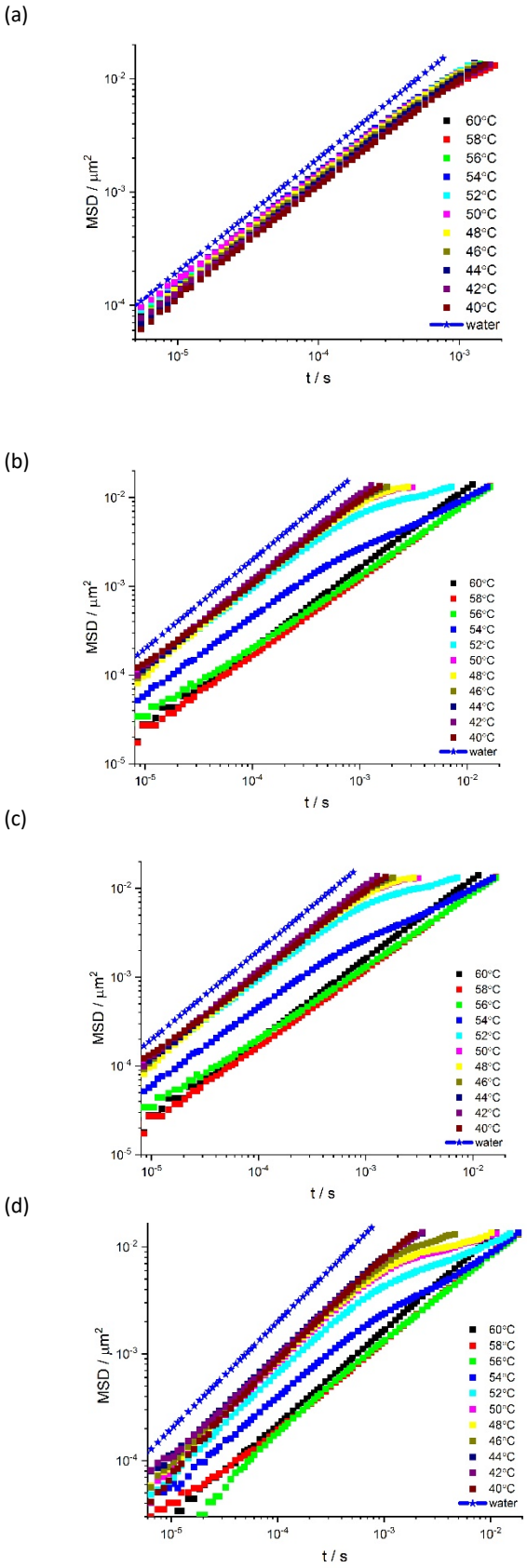

Fig. S4 Ensemble-averaged MSD for PS-PEG colloids diffusing under Brownian motion in (a) 0.8%w, (b) 1.0%w, (c) 1.6%w and (d) 2.0%w solutions containing a 2:3 ratio of Y-shapes and L6 linkers with flexible joints. The curves are plotted as functions of lag time and the legend indicates the temperature, at which each curve is generated.

Flexible linkers

Figure S4 shows the MSD curves for the same total DNA concentration and temperature range as in Figure S3, but for hydrogels assembled using flexible linkers. At high temperatures and low concentrations (0.8%w and 1.0%w), the MSD curves look very similar to the ones for the rigid linker case. However, as the temperature is lowered, the increase in viscosity using L0 linkers is significantly larger. The introduced flexibility by inserting six thymine bases in the free joint appears to slow down gelation and thus the viscosity remains roughly the same throughout the studied temperature range.

Particularly intriguing are the MSD curves corresponding to highly concentrated flexible hydrogels. In agreement with the g_1 curves shown in the main body of the paper, the viscosity appears to decrease on lowering the temperature, contrary to our initial expectations. We aim to explain this behavior through the formation of a cluster phase that contains some flexible linkers and Y-shapes connected as in the rigid linker case (Figure 2(a)) and some connected in the way shown in Figure 2(b). This new type of connectivity can lead to the formation of large voids, where the PS-PEG colloids are expelled and as a result sense on average lower viscosity than at higher temperatures. However, none of our samples displayed macroscopic phase separation, which is in agreement with existing theories predicting the phase behavior of DNA hydrogels of various valency.

Relaxation times

Fernandez-Castanon *et al.* also report the characteristic relaxation times extracted from their measured DLS data for X-shaped nanostars. They present the relaxation time distributions associated with the corresponding scattering autocorrelation functions, using their CONTIN regularisation algorithm. In Fig. S5 we present the relaxation times associated with the obtained scattering functions measured for the Y-L0 and Y-L6 systems, which we present in Fig. 2 of the main article. These relaxation time distributions were obtained using our in-house developed regularisation method.

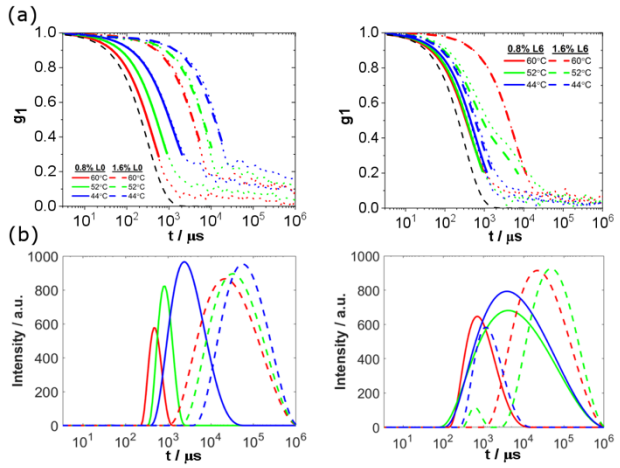

Fig. S5 (a) Intermediate scattering functions above, around and below melting for the rigid (L0) and flexible (L6) linker hydrogels at concentrations of 0.8%w and 1.6%w. (b) Time relaxation distributions corresponding to the intermediate scattering functions in (a), obtained from CONTIN analysis.

Different to Fernandez-Castanon *et al.*, we do not see the emergence of a second relaxation time at percolation for the Y-L0 system, which also coincides with the system's meting temperature $T_{m,L0(6)} \approx$ 52-54°C. However, a clear broadening of the relaxation time peak below $T_{m,L0(6)}$ is noticeable. We argue that this broadening simply reflects the fact that although the system is percolating, not all bonds have formed and different not yet connected clusters or loose parts of the gel contribute to the relaxation times of the bulk.

Interestingly, only the Y-L6 sample shows a second, small peak at shorter times that most likely stems from the relaxation modes of the clusters formed below $T_{m,L0(6)}$. We argue that the difference between our data and those presented by Fernandez-Castanon *et al.* are due to the difference in the type of CONTIN algorithm used. Indeed, when using the commercial CONTIN analysis provided by the Malvern machine, we do obtain several peaks in the relaxation time distribution, which we account for incorrect evaluation of noisy data.

Bulk rheology

We performed conventional bulk rheology in an attempt to confirm our microrheology results from DLS. We used a Kinexus Pro+ rheometer (Malvern Instrument, stress and strain control), equipped with a parallel-plate geometry (8-mm diameter and fixed gap of 0.15 mm). We used a 40 µL sample volume in each measurement. Time-sweep tests were carried out at a fixed strain of 1% and fixed frequency of 1 Hz at 25 °C (not shown here). Frequency-sweep tests were carried out between 10 Hz and 0.01 Hz and a fixed strain of 1%. The temperature for the frequency sweeps was ramped from 15°C to 60°C in increments of 5°C.

Figures S6 and S7 show the viscoelasticity of 0.8%w, 1.0%w and 1.6%w hydrogels made of 2:3 ratios of Y-shapes and L0 linkers at 50°C and 15°C, respectively. The formation of the gel at low temperatures is evident from the order of magnitude difference between G' and G''. This difference is maintained at even higher temperatures until around 40°C we observe a decrease in G' accompanied by an increase in G''. In complete agreement with our expectations, increasing the concentration of total DNA in the test sample results in the formation of a stronger gel at low temperatures. We successfully confirm that the melting temperature of our hydrogel is around 50°C, where the loss modulus starts to overcome the storage modulus and the sample turns into liquid. There is a slight shift in the melting temperature $T_{m,L0(6)}$ with total DNA concentration c, which is expected from classical nucleic acid thermodynamics, where T_m scales as $(\ln c)^{-1}$. This shift in $T_{m,L0(6)}$ is also observed in our DLS measurements, reported in the main body of the manuscript.

Performing measurements on the flexible linker hydrogels proved unsuccessful as there was a large scatter in the data due to reaching the sensitivity limit of the instrument. This result on its own, however, can serve as a confirmation that the gel truly does not form when L6 flexible linkers are used.

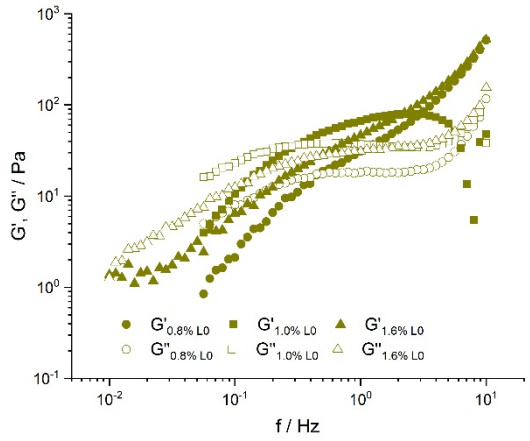

Fig. S6 Bulk rheology measurements at 50°C for three total DNA concentrations of rigid linker hydrogel: 0.8%w (circles), 1.0%w (squares) and 1.6%w (triangles). Storage moduli are shown with filled symbols, while empty symbols represent loss moduli.

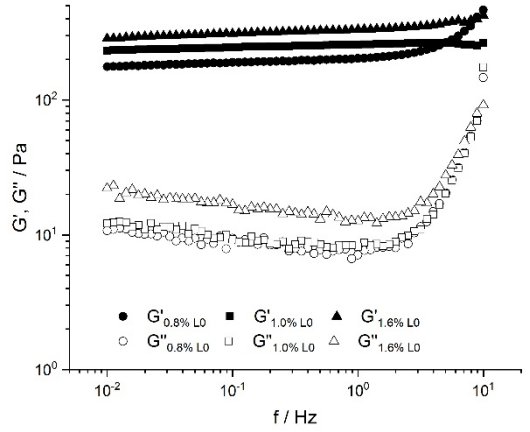

Fig. S7 Bulk rheology measurements at 15°C for three total DNA concentrations of Y-L0 hydrogels: 0.8%w (circles), 1.0%w (squares) and 1.6%w (triangles). Storage moduli are shown with filled symbols, while empty symbols represent loss moduli.

OxDNA Simulations

We performed oxDNA simulations to verify that when using linear linkers with flexible joints, it is possible to create a loop between a Y-shape and a linker, having the sequences specified in Table 1 of the manuscript. Videos SV1 and SV2 follow the diffusion of the nanostar-linker assembly in the rigid and flexible linker case scenarios, respectively. On careful inspection of the videos, one can gain an idea of the effect that flexibility has on the range of accessible angles achieved by the assembly. These were indeed the videos analyzed in order to obtain the result reported in Figure 1 of the manuscript. The closing of the ring and the loop formation in the case of using flexible linkers is illustrated clearly.

In Fig. S8, we also present the angle distributions between a rigid arm of a Y-shape bound to a linear linker with either 0, 2, 4 or 6T long flexible joints. As can be seen, the 4T and 2T long joints of linkers L4 and L2, respectively, show a peak shift in their preferred angles θ towards smaller values. This signifies that in order for a single L4 or L2 linker to bind to two arms of the same Y-shape, it needs to pull the two arms closer together, demanding an increasing bending energy penalty the system has to pay. Below we estimate the value of the penalty.

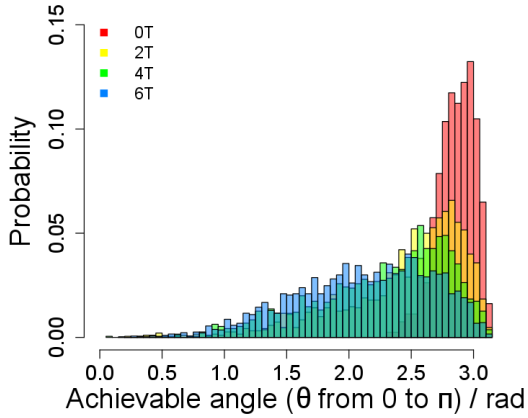

Fig. S8 Simulations on oxDNA of the angle distributions of angle θ between the rigid arm of a Y shape and a L0 (red), L2 (yellow), L4 (green) and L6 (blue) linker with 0, 2, 4 and 6 thymines, respectively. All simulations were performed at 25°C.

Computing the Bending Energy

The bending free energy cost for binding a linker to two arms of the same Y-shape can be computed by first evaluating the average equilibrium angles between the tree arms of a free Y-shape. We name these angles α_1, α_2 and α_3. Their probability distributions in a Y-L6 system, obtained from long oxDNA simulation runs at 25°C, are plotted in Fig. S9. As expected, the individual mean angles are similar. This changes when two arms are connected with an L6 linker.

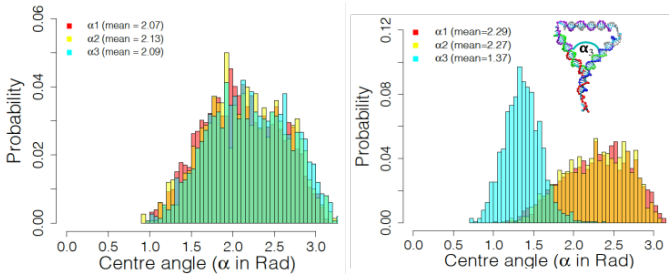

Fig. S9 (*left*) Probability distributions of the three angles α_1, α_2 and α_3 between the three arms of a free Y-shape, obtained from oxDNA simulations. (*right*) Change of the angle distributions after attaching a L6 linker with 6 thymine joints.

We can compute the penalty in the total free energy of the free and connected Y-shapes through $F(\alpha) = -k_BT \ln(P(\alpha))$. Plotting both in Fig. S10 we can read off that the bending free energy must be of the order of 0.5 k_BT. The binding free energy between the sticky arms of the Y-shape and the linear linker, however, is about 23.5 k_BT. The bending energy increases rapidly when the free joint is reduced to 4T or 2T. Starting out with a closed configuration at room temperature

in the oxDNA simulations shows a rapid unbinding of one linker arm from the Y-shape.

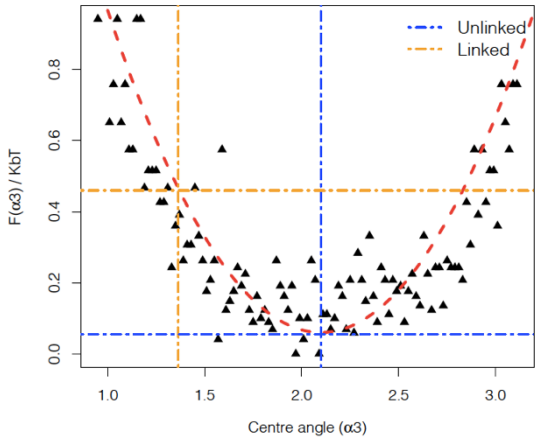

Fig. S10 Free energy as function of the angle distribution between the free arms in a Y-shape (parabola) and the free energy of a Y-shape connected via a L6 linker at the mean angle of this configuration (yellow vertical line).

References

1 L. Di Michele, B. Mognetti, T. Yanagishima, P. Varilly, Z. Ruff, D. Frenkel and E. Eiser, 'Effect of inert tails on the thermodynamics of DNA hybridization,' *J. Am. Chem. Soc.*, 2014, **136**, 6538–6541.

2 H. T. Allawi and J. SantaLucia, 'Thermodynamics and NMR of internal G·T mismatches in DNA,' *Biochemistry*, 1997, **36**, 10581–10594.

3 Z. Xing, A. Caciagli, T. Cao, I. D. Stoev, M. Zupkauskas, T. O'Neill, T. Wenzel, R. Lamboll, D. Liu and E. Eiser, 'Microrheology of DNA hydrogels,' *Proc. Natl. Acad. Sci.*, 2018, **115**, 8137–8142.